Published in final edited form as:
J Am Chem Soc. 2013 July 3; 135(26): 9665–9674. doi:10.1021/ja312571m.

Spectroscopic Studies of the Mononuclear Nonheme Fe^{II} Enzyme FIH: Second–Sphere Contributions to Reactivity

Kenneth M. Light[†], **John A. Hangasky**[‡], **Michael J. Knapp**[‡], and **Edward I. Solomon**[*,†]

[†]Department of Chemistry, Stanford University, Stanford, CA 94305

[‡]Department of Chemistry, University of Massachusetts, Amherst, MA 01003

Abstract

Factor Inhibiting Hypoxia–Inducible Factor (FIH) is an α-ketoglutarate (αKG) dependent enzyme which catalyzes hydroxylation of residue Asn803 in the C-terminal transactivation domain (CAD) of hypoxia–inducible factor 1α (HIF-1α) and plays an important role in cellular oxygen sensing and hypoxic response. Circular dichroism (CD), magnetic circular dichroism (MCD) and variable–temperature, variable–field (VTVH) MCD spectroscopies are used to determine the geometric and electronic structures of FIH in its (Fe^{II}), (Fe^{II}/αKG) and (Fe^{II}/αKG/CAD) forms. (Fe^{II})FIH and (Fe^{II}/αKG)FIH are found to be six-coordinate (6C), whereas (Fe^{II}/αKG/CAD)FIH is found to be a 5C/6C mixture. Thus, FIH follows the general mechanistic strategy of nonheme Fe^{II} enzymes. Modeling shows that when Arg238 of FIH is removed the facial triad carboxylate binds to Fe^{II} in a bidentate mode with concomitant lengthening of the Fe^{II}–αKG-carbonyl bond, which would inhibit the O_2 reaction. Correlations over α-keto acid-dependent enzymes and with the extradiol dioxygenases shows that members of these families (where both the electron source and O_2 bind to Fe^{II}) have a second-sphere residue H-bonding to the terminal oxygen of the carboxylate, which stays monodentate. Alternatively, structures of the pterin-dependent and Rieske dioxygenases, which do not have substrate binding to Fe^{II}, lack H-bonds to the carboxylate, and thus allow its bidentate coordination which would direct O_2 reactivity. Finally, Vis-UV MCD spectra show an unusually high-energy $Fe^{II}\rightarrow$αKG π* metal-to-ligand charge transfer transition in (Fe^{II}/αKG)FIH which is red-shifted upon CAD binding. This red shift indicates formation of H bonds to the αKG that lower the energy of its carbonyl LUMO, activating it for nucleophilic attack by the Fe-O_2 intermediate formed along the reaction coordinate.

Introduction

Oxygen-activating mononuclear nonheme iron enzymes catalyze the reactions of a wide variety of organic substrates with O_2 with relevance to health, pharmaceutics, and environmental remediation.[1, 2] These enzymes utilize an Fe^{II} center which directly binds O_2 to form iron-oxygen intermediates competent for reaction with substrate. As the one–electron reduction of O_2 to form a Fe^{III}-O_2^- species is thermodynamically unfavorable,[3] these enzymes also utilize a cofactor or redox-active substrate as a source of the additional electrons needed for O_2 activation. The majority of Oxygen-activating mononuclear nonheme iron enzymes may be divided into four families based on the source of additional electrons to generate the oxidizing intermediate.[4] Rieske dioxygenases utilize one electron from a Rieske [2Fe-2S] cluster close to the mononuclear active site and connected through a hydrogen-bond (H-bond) network. Pterin-dependent hydroxylases require a

[*]**Corresponding Auther:**edward.solomon@stanford.edu.

Supporting Information **Available:** DFT geometry optimization procedure, additional CD spectra of CAD binding, table of DFT thermodynamics, coordinates for all optimized structures, additional pictures of FIH crystal structures, and full reference 35.

tetrahydrobiopterin (BH_4) cofactor bound in the active site pocket, though not covalently bound to Fe^{II}. Extradiol dioxygenases coordinate catecholate substrates to Fe^{II} in a bidentate fashion and catalyze their ring cleavage (the catecholate providing the extra electrons required for reactivity). α-ketoglutarate-dependent (αKG-dependent) oxygenases use a coordinated αKG which binds bidentate to Fe^{II}. All four of these families utilize a 2-His-1-carboxylate facial triad motif of amino acid derived ligands for Fe complexation.[5-7]

Factor Inhibiting Hypoxia-Inducible Factor, FIH, is an αKG-dependent asparaginyl hydroxylase involved in sensing hypoxia within the cells of humans and other animals.[8] Its substrate is the C-terminal activation domain (CAD) of the Hypoxia-Inducible Factor 1α (HIF-1α), one subunit of a heterodimeric transcription factor protein. HIF-1α controls over 100 genes involved in increased O_2 delivery to the cell, including those associated with production of erythropoietin for increased red blood cell production and vascular endothelial growth factor, which is a major stimulant for angiogenesis.[9-12] As long as sufficient O_2 is present, FIH will hydroxylate Asn803 of HIF-1α. This hydroxylation prevents binding of the transcriptional co-activators p300 or CPB (**C**yclic adenosine monophosphate response element-**B**inding-**P**rotein) to HIF-1α which is required for gene activation.[13-15] Once O_2 concentrations within the cell drop to a sufficient level, Asn803 of HIF-1α is no longer hydroxylated and the hypoxic response commences. Although HIF-1α is composed of over 800 residues and has not been made in sufficient quantity for biochemical studies, a CAD fragment containing approximately 40 residues has been shown to be hydroxylated by FIH at the appropriate position in Asn803.[16, 17] The relatively small size of this substrate compared to the full protein may lead to the deletion of a number of substrate-enzyme interactions which as of this time have not been tested, and increasing the size of the CAD substrate does have an effect on k_{cat} and K_m.[18] However, FIH can hydroxylate the CAD fragment *in vitro* on a reasonable timescale (20 minutes) at the correct position of Asn803 with >10:1 coupled:uncoupled turnover[15] indicating that this truncated substrate is a reasonable model for biochemical studies.

αKG-dependent enzymes follow a general mechanistic strategy in which the Fe^{II} site is six-coordinate (6C) when the active site is devoid of substrate or αKG cofactor (in its "resting" form), the Fe^{II} being coordinated to the facial triad and three water ligands. αKG displaces two of the water ligands to coordinate bidentate to the Fe^{II}. In this form the site remains 6C, which limits reaction of the Fe^{II} αKG site with O_2 before substrate is in position. Substrate binding leads to release of the remaining water ligand, thereby opening a coordination site for reaction with O_2.[19, 20] For example, in the case of halogenase SyrB2 the rate of reaction of the substrate-bound complex with O_2 is ≈ 5000 times faster than that of the substrate-free form.[21] Another example from a different nonheme Fe^{II} enzyme family is found in the pterin–dependent enzyme tyrosine hydroxylase, where the rate of O_2 binding to the 5C pterin/substrate-bound form is ≈ 200 times faster than that of the 6C site in the absence of substrate.[22] Reaction with O_2 before substrate and cofactor are in place can lead to uncoupled turnover as well as self-hydroxylation of the enzyme which has been observed in several αKG-dependent proteins when αKG is bound and substrate is absent.[23-25] In the case of 1-aminocyclopropane-1-carboxylic acid oxidase (ACCO) binding of 1-aminocyclopropane-1-carboxylic acid in the absence of CO_2/HCO_3^- leads to a 5C site[26] which reacts with O_2 to form Fe^{III} and generates almost no ethylene product.[27] In the presence of CO_2/HCO_3^- the site will remain 6C until the cofactor ascorbate also binds.[26] These findings point to the importance of forming a 5C Fe^{II} site only when all of the necessary components are in place for coupled reaction.

The active site of αKG/CAD-bound FIH ((Fe^{II}/αKG/CAD)FIH) as determined by crystallography is shown in Figure 1[16] where the key second-sphere interactions are hydrogen bonds from the backbone amide of Asn803 of CAD and from the sidechain of FIH

Arg238. In this figure the majority of CAD C atoms are colored yellow. Asn803 of the CAD substrate is held in place above the Fe^{II} through H-bonds with FIH residues Arg238 and Gln239 as shown in Figure 1A. The β-carbon of CAD Asn803 (colored magenta) is the target for hydroxylation and is poised directly above the Fe^{II} atom. The CAD Val802-Asn803 backbone amide N-H group H-bonds with the facial triad carboxylate as shown in Figure 1B. In the absence of substrate, H-bonding between the facial triad carboxylate and the coordinated water in the αKG-bound form of αKG-dependent enzymes strengthens the Fe-OH_2 bond by giving the water partial hydroxide character.[28] When this H-bond cannot be formed, such as in TauD where the carboxylate of the facial triad is tilted down and in the halogenases CytC3 and SyrB2 which have halide ions in place of the facial triad carboxylate, an alternative enzyme residue H-bonds to coordinated water which helps keep it bound to the Fe^{II} active site.[28] In CAD-bound FIH, the substrate amide-facial triad carboxylate H-bond may therefore serve a purpose in weakening the Fe-OH_2 bond by competing with the coordinated water for the facial triad carboxylate O not coordinated to Fe^{II} and thus help induce water loss. The contributions of substrate H-bonding and steric clashes to loss of coordinated H_2O in NH Fe^{II} enzymes will be presented elsewhere.[29] It is also interesting to note that the facial triad carboxylate is tilted towards Arg238 both in the presence and absence of CAD substrate (Figure 1B). This carboxylate orientation implies an additional H-bond interaction, which also may serve to weaken the carboxylate-water H-bond mentioned above.

In contrast to the general mechanistic strategy described above, crystal structures for (Fe^{II}/αKG)FIH in the absence of CAD do not give definitive evidence for the presence or absence of a coordinated water ligand.[16, 30] EPR spectroscopic studies of (Co^{II}/aKG)FIH indicated that this form is a 5C/6C mixture.[25] Such behavior has not been observed for other members of the family and a 5C (Fe^{II}/αKG)FIH site would lead to uncoupled turnover and potential deactivation of the enzyme. Our laboratory has developed a methodology utilizing near-infrared (NIR) circular diochroism (CD), magnetic circular dichroism (MCD) and variable-temperature, variable-field (VTVH) MCD spectroscopies to obtain detailed ligand field information about the geometric and electronic structures of Fe^{II} sites in proteins in solution.[31, 32] In the present study this methodology (outlined at the beginning of the Results section) has been utilized to evaluate the mechanistic strategy of FIH in comparison to other αKG-dependent enzymes. We have also used Vis/UV MCD spectroscopy to obtain insight into the metal-to-ligand charge transfer (MLCT) transitions present for the αKG-bound forms of members of this enzyme family, most notably clavaminate synthase 2 (CS2).[28, 33, 34] Vis/UV MCD spectroscopy has been used here to analyze the electronic structures of the αKG- and αKG/CAD-bound forms of FIH which show large differences relative to the other αKG enzymes studied and coupled with density functional theory (DFT) calculations provide insight into how second-sphere interactions tune the reactivity of the Fe^{II}-αKG moiety towards reaction with O_2. These calculations also provide important new insight into how the second-sphere Arg238 interaction in Figure 1B tunes the reactivity of the Fe^{II} active site both specifically in FIH and generally over all four classes of Oxygen-activating nonheme iron enzymes.

Materials and Methods

Sample Preparation

Recombinant human FIH and HIF-1α CAD 39-mer were expressed and purified as described previously.[25] The CAD substrate corresponded to human HIF-1α residues 788-826, with a C800A point mutation to prevent spurious oxidation reactions: DESGLPQLTSYDAEV**N**APIQGSRNLLQGEELLRALDQVN. The CAD peptide was purchased as a desalted peptide from EZBiolab (Carmel, IN, USA) with free N and C-

termini. RP-HPLC utilizing a gradient from 30% acetonitrile/0.1% trifluoroacetic acid (TFA) to 95% acetonitrile/0.1% TFA was used to obtain CAD of >95% purity. Apo-FIH was exchanged into deuterated HEPES buffer (50 mM, pD 7.5) to a concentration of 8–9 mM active sites (4–5 mM enzyme homodimers). CAD substrate was lyophilized for storage and added to samples of FIH in this form. Samples for spectroscopy were prepared in an anaerobic "wet box" under N_2 atmosphere. Ferrous ammonium sulfate and αKG were added in microliter quantities from anaerobic stock solutions in degassed D_2O and deuterated HEPES buffer, respectively. For cofactor and substrate binding, aliquots were added until no further spectral change was observed. Enzyme samples were saturated with sucrose for preparation of MCD cells to final enzyme-bound Fe^{II} concentrations of 8–9 mM active sites. CD spectra were taken without and with sucrose addition to ensure that the glassing agent did not perturb the Fe^{II} site.

Spectroscopic Methods

NIR (600–2000 nm) CD and MCD data were recorded on a JASCO J-730 spectropolarimeter with a liquid N_2-cooled InSb detector and an Oxford Instruments SM4000-7T superconducting magnet. Vis-UV (300–900 nm) MCD data were recorded on a JASCO J-810 spectrapolarimeter with an extended S-20 photomultiplier tube and an Oxford Instruments SM4000-7T superconducting magnet. CD spectra were corrected for buffer and cell contributions, and MCD spectra were corrected for the natural CD and zero-field baseline effects by averaging the magnitudes of the positive and negative field data. VTVH MCD data were collected with a calibrated Cernox resistor (Lakeshore Cryotronics, calibrated from 1.5–300 K) inserted into the sample cell for accurate sample temperature measurement. VTVH MCD data were normalized to the intensity maximum over all isotherms for a given wavelength, and ground state parameters were obtained by fitting the data as previously described.[31, 32]

Computational Methods

The active site of αKG–bound FIH was modeled using the crystal structure with PDB ID 1H2N as the starting point.[16] The active sites was truncated and key carbon coordinates frozen as described in the Supporting Information. DFT and time dependent DFT (TD-DFT) calculations were performed on all active site structures using the Gaussian 09 software package.[35] Geometry optimizations and single point calculations were conducted using the spin-unrestricted BP86 functional with 10% Hartree–Fock mixing, and TD-DFT calculations were performed using the spin-unrestricted B3LYP functional. All calculations were performed under tight convergence criteria. The triple–ξ basis set 6–311G* was used to describe the Fe atom, the N and O atoms of the facial triad directly coordinated to Fe, the O atom of coordinated water, and the OC–CO_2 moiety of coordinated αKG, while all other atoms were modeled using the double–ξ basis set 6–31G*. Solvation effects were included in all calculations through the use of the polarized continuum model (PCM)[36] with a dielectric constant ε = 4.0. Atomic Cartesian coordinates for all optimized structures are provided in the Supporting Information.

Results

In the results presented below we use CD and MCD spectra taken in the near-infrared (NIR) region to detect Fe^{II} ligand field (LF) transitions that are weak and otherwise obscured by water and protein vibrational transitions in absorption spectroscopy. An analysis of the NIR MCD spectra of a series of 6C, 5C, and 4C model complexes developed in reference 32 has allowed for the determination of the coordination geometry around Fe^{II} based on the energies and splitting patterns of the LF transitions. Fe^{II} in a biologically relevant ligand coordination environment of octahedral symmetry possesses a $^5T_{2g}$ ground state and ^5E_g

excited state that are split in energy by 10 Dq ≈ 10000 cm^{-1}. 6C sites in lower than octahedral symmetry (i.e. the facial triad and three water ligands) generally show two LF transitions centered around 10000 cm^{-1} (i.e. 10 Dq) and split by $\Delta^5E_g \approx 2000\ cm^{-1}$. Removal of one ligand to form a 5C square pyramidal site leads to a transition at ≈ 5000 cm^{-1} and one above 10000 cm^{-1}. Alternatively, a 5C trigonal bipyramidal site shows one transition at less than 5000 cm^{-1} (frequently undetectable) and another at less than 10000 cm^{-1}. A 4C tetrahedral site shows only LF transitions centered around 6000-7000 cm^{-1} due to the significantly smaller values of 10 Dq for tetrahedral vs. octahedral complexes ($10Dq\,(T_d) = -\frac{4}{9}10Dq\,(O_h)$). No single Fe^{II} site exhibits more than two CD/MCD bands in the NIR region. NIR CD and MCD spectra are therefore good indicators of coordination geometry and whether or not a mixture of Fe^{II} species is present. Further, NIR VTVH MCD spectroscopy (i.e. the MCD amplitude at a given wavelength as a function of field for a fixed series of increasing temperatures plotted against βH/2kT) provides information about the ground-state splitting of the t_{2g} orbitals for a given site. A non-Kramers doublet model has been developed for the fitting of VTVH MCD data which provides ground state spin Hamiltonian parameters δ and $g_{\|}$ which in turn are used to determine the tetragonal splitting, Δ, of the d_{xy} orbital from the {d_{xz}, d_{yz}} pair, as well as the rhombic splitting, V, of the d_{xz} and d_{yz} orbitals.[31] This splitting of the dπ orbitals can therefore be fully characterized and in combination with the CD/MCD transition energies gives a complete picture of the active site geometric and electronic structure.

NIR CD and MCD spectra for (Fe^{II})FIH, (Fe^{II}/αKG)FIH and (Fe^{II}/αKG/CAD)FIH are given in Figure 2.

The 283 K CD spectrum of (Fe^{II})FIH (Figure 2A, blue) contains two transitions at ≈ 8000 and 11400 cm^{-1} (negative). Upon cooling to 1.8 K the transitions sharpen and shift to approximately 9100 and 10900 cm^{-1} as shown in the 7 T MCD spectrum of resting FIH (Figure 2B, blue). The observed Δ^5E_g of 1800 cm^{-1} is typical of 6C resting αKG-dependent enzymes. Although the bands shift significantly in energy upon going from 283 K to 5 K, similar behavior has been observed for the enzyme CS2 and has been attributed to stronger Fe-OH_2 bond interactions at lower temperature (the Δ^5E_g for CS2 goes from ≈ 2400 cm^{-1} in the room temperature CD spectrum to ≈ 1700 cm^{-1} in the 5 K MCD spectrum).[33]

Addition of 20 equivalents of αKG to (Fe^{II})FIH produces the αKG-bound form. Both the 283 K CD and 1.8 K/7 T MCD spectra (Figure 2A, red and 2B, red, respectively) show two transitions in the ligand field region centered around 10000 cm^{-1} split by ≈2000 cm^{-1}, which imply that (Fe^{II}/αKG)FIH possesses a 6C site. While the 8400 and 11300 cm^{-1} transitions in the CD spectrum at 283 K are similar to those of (Fe^{II})FIH, the Δε values of the (Fe^{II}/αKG)FIH transitions are appreciably larger in magnitude. At low temperature these transitions are shifted to 8900 and 11200 cm^{-1} in the MCD spectrum. The larger band splitting observed in low-temperature MCD spectra for (Fe^{II}/αKG)FIH *vs* (Fe^{II})FIH (Δ^5E_g ≈ 2300 cm^{-1} for αKG-bound *vs* 1800 cm^{-1} for resting) is consistent with a weakening of the remaining Fe^{II}-OH_2 bond upon binding of αKG, which is a stronger donor than the two water ligands it displaces. Also visible in the MCD spectrum of (Fe^{II}/αKG)FIH is an intense positive tail on the high-energy side which comes from an Fe^{II} dπ to αKG π* metal-to-ligand charge transfer (MLCT) transition centered at ≈ 20000 cm^{-1}. (*vide infra*)

Addition of 1.7 equivalents of CAD substrate (97% loading, see Supporting Information) to (Fe^{II}/αKG)FIH produces the αKG/CAD-bound form. The CD spectrum taken at 283 K (Figure 2A, green) now has a new feature at low energy (<6000 cm^{-1}), which indicates that a square pyramidal 5C species is present in the sample. From the 3 K MCD spectrum (Figure 2B, green) three resolved peaks are visible: a low energy feature corresponding to

the shoulder in the CD spectrum at ≈ 5500 cm^{-1} and peaks at ≈ 8000 cm^{-1} and 11200 cm^{-1}. The spectrum cannot be fit without inclusion of a 4th peak at ≈ 9000 cm^{-1} as shown in Figure 2C. The energy positions of these four features (one low energy and three higher energy LF transitions) require that (Fe^{II}/αKG/CAD)FIH is a 5C/6C mixture of two species. While one might initially consider from MCD peak positions that some unconverted αKG-bound enzyme remains, the peak area ratios of the ≈ 9000 to 11200 cm^{-1} features do not match between the two spectra; for the spectrum of αKG-bound FIH, the ratio is approximately 1:1 (orange dashed lines, Figure 2C), whereas for αKG/CAD-bound FIH it is closer to 2:3 (blue dashed lines).

VTVH MCD data were collected for resting, αKG-bound and αKG/CAD-bound FIH and are shown in Figure 2D, 2E, and 2F respectively. The saturation magnetization behavior for (Fe^{II})FIH at ≈ 8200 cm^{-1} (blue arrow in Figure 2B; note the energy used for VTVH is offset from the peak maximum to avoid overlap with the higher energy peak) is well fit with ground-state spin Hamiltonian parameters $\delta = 3.9 \pm 0.2$ cm^{-1} and $g_{\|} = 9.2 \pm 0.1$ which correspond to $\Delta = -275 \pm 50$ cm^{-1} and $|V/2\Delta| = 0.19 \pm 0.02$. These small $^5T_{2g}$ ground-state splittings are very similar to those observed for the resting forms of other α-keto acid dependent enzymes, where none of the ligands have particularly strong π interactions with the metal.[28, 33, 37] Comparison of ΔE_g values, Data were chosen for the (Fe^{II}/αKG/subst.) form of CS2 with deoxyguanidinoproclavaminic acid (DGPC) bound.[26, 28] The data for the 8900 cm^{-1} peak of (Fe^{II}/αKG)FIH taken at ≈ 8200 cm^{-1} (red arrow in Figure 2B) are well fit by the parameters $\delta = 2.8 \pm 0.2$ cm^{-1} and $g_{\|} = 8.9 \pm 0.1$ corresponding to a $\Delta = -950 \pm 50$ cm^{-1} and $|V/2\Delta| = 0.28 \pm 0.02$. The increased $^5T_{2g}$ ground-state splitting is caused by the αKG ligand which has a strong π-back-bonding interaction with the Fe^{II} ion as found previously for other α-keto-dependent enzymes.[28, 33, 37]

The data for the 8000 cm^{-1} peak of (Fe^{II}/αKG/CAD)FIH taken at ≈ 7550 cm^{-1} (green arrow in Figure 2B) is fit with $\delta = 1.8 \pm 0.2$ cm^{-1} and $g_{\|} = 9.2 \pm 0.1$ corresponding to a $\Delta = -1200 \pm 100$ cm^{-1} and $|V/2\Delta| = 0.17 \pm 0.02$. Note that from Figure 2 D to E to F the nesting of the VTVH MCD data decreases as Δ increases. This large magnitude of Δ relative to that of (Fe^{II}/αKG)FIH is consistent with a 5C square pyramidal αKG-bound site indicating loss of water upon αKG and substrate binding. VTVH data taken at ≈ 9400 cm^{-1} for CAD/αKG-bound FIH could not be fit to any single set of parameters due to overlap with other more intense bands.

Vis–UV MCD spectra of (Fe^{II}/αKG)FIH and (Fe^{II}/αKG/CAD)FIH (red and green curves, respectively) are given in Figure 3, along with those of (Fe^{II}/αKG)TauD and (Fe^{II}/αKG/taurine)TauD (black and purple, respectively) for comparison.[28]

The major feature in each spectrum at ≈ 20000 cm^{-1} corresponds to an Fe^{II} dπ to αKG π* MLCT transition.[33] The $\tilde{\nu}_{max}$ of αKG-bound FIH is abnormally high at 20700 cm^{-1}. Addition of CAD substrate red-shifts $\tilde{\nu}_{max}$ to 20000 cm^{-1}. This trend is opposite of that observed for TauD, which shows a blue-shift in $\tilde{\nu}_{max}$ upon taurine binding: (Fe^{II}/αKG)TauD and (Fe^{II}/αKG/taurine)TauD exhibit $\tilde{\nu}_{max}$ values of 18800 and 19200 cm^{-1}, respectively. This shift of the MLCT to higher energy upon binding of substrate is commonly observed for other αKG-dependent enzymes, and has been attributed to strengthening of the Fe^{II}-αKG bond upon loss of coordinated water.[20, 28, 38] The origin of the unusual MLCT energies in FIH and consequent implications for O_2 reactivity will be explored in the Analysis and Discussion sections, respectively.

Analysis

Second-Sphere Interactions with the Facial Triad: Mono- vs Bidentate Coordination—From the above spectroscopic studies a H_2O is lost from the αKG-bound

Fe^{II} site upon CAD substrate binding. In crystal structures of FIH (Figure 1B) the facial triad carboxylate is tilted so that its non-bonding O is pointed at the positively-charged Arg238 of FIH, implying a second-sphere interaction between the two residues and a weakening of the carboxylate-ligated water H-bond which would allow the H_2O to more easily dissociate from the Fe^{II} site. In order to explore this effect on the active site, DFT computational models were constructed and their geometries optimized as shown in Figure 4 wherein Arg238 is either in its crystallographic position or moved away from the active site (by ≈ 40 Å) to minimize its interaction with the carboxylate of the facial triad. Figure 4A shows that for 6C FIH the facial triad carboxylate is tilted toward positively charged Arg238 when the latter residue is in its crystallographic position. Displacement of Arg238 as in Figure 4B causes the carboxylate to tilt so as to better H-bond with the ligated water (the carboxylate O/water H distance decreases by ≈ 0.1 Å). This implies that the presence of Arg238 should aid in water loss, and 5C models where the coordinated water was removed were geometry-optimized so that the effect of Arg238 could be determined (Figures 4C and 4D). An important result for the 5C forms was found: Whereas 5C FIH with Arg238 in its crystallographic position as shown in Figure 4C retains a monodentate carboxylate ligand (and is 5C as experimentally observed above), displacement of Arg238 from the active site in the absence of coordinated water leads to bidentate ligation for the facial triad carboxylate, and the Fe^{II}-αKG carbonyl bond weakens from ≈ 2.2 Å to 2.4 Å (Figure 4D). Bidentate coordination in the absence of an H-bonding partner was also observed computationally for prolyl hydroxylase domain containing protein PHD2.[39] This finding has important implications for αKG-dependent enzymes in general and is relevant to all four classes of NH Fe^{II} enzymes. These implications are explored in the Discussion section.

Second-Sphere Interactions with the αKeto Acid: Effects on the MLCT transition—The MLCT transitions of (Fe^{II}/αKG)FIH and (Fe^{II}/αKG/CAD)FIH are significantly higher in energy than those of other αKG-dependent enzymes, and the downshift in energy upon substrate CAD binding is the opposite of what is observed for other members of the family (as seen in Figure 3). Changes in MLCT energies are due to shifts in the energies of either the donor (Fe^{II} t_{2g}) or acceptor (αKG π*) orbitals, both of which have an effect on the reactivity of the active site. In order to determine the cause of the unusual MLCT energies of (Fe^{II}/αKG)FIH and energy downshift of (Fe^{II}/αKG/CAD)FIH as well as implications for reactivity, the crystal structures for FIH as well as two other αKG-dependent enzymes, CS2[40] and TauD,[41] were examined to determine differences in local environments around the αKG-Fe^{II} moiety. One particularly interesting structural feature of both CS2 and TauD is that the arginine, which in FIH (Arg238) is H-bonding with the facial triad carboxylate (Figure 5A) is instead located near and H-bonding with the carboxylate of the coordinated αKG, as can be seen for the CS2 structure shown in Figure 5B (Arg297).

To explore the effects of αKG carboxylate H-bonding on MLCT energy, TD-DFT calculations were performed with Arg238 in its crystallographic position (as in Figure 5A) and a model where this residue was shifted to H-bond with αKG as in TauD and CS2 (Figure 5B). The calculated transition energies for the H_2O–ligated 6C forms for both models are given in Table 2A.

Comparison of 6C forms with Arg238 in the FIH *vs* the CS2/TauD position shows that the MLCT of the former is higher in energy by ≈2500 cm^{-1}, similar to the difference in MLCT energies between FIH and TauD (≈1900 cm^{-1} in Figure 3). This red-shift in the MLCT transition with H-bonds to the αKG reflects the stabilization of the αKG π* orbital. Also as can be seen for both models in Table 2B and 2C, the loss of water increases the MLCT energy by ≈1600 cm^{-1}. This blue-shift of the MLCT has been experimentally observed for TauD[20, 28] and is due to the loss of the water ligand causing the Z_{eff} of Fe^{II} to increase, thus

shifting the d orbital manifold down in energy, though the experimental shift is significantly smaller in magnitude (400 cm^{-1}) than that calculated (1600 cm^{-1}). However, a shift in the opposite direction is observed for FIH (Figure 3), as binding the CAD substrate with the associated loss of the water ligand causes the MLCT transition to shift down in energy.

From crystallography on FIH, there appears to be a change in H-bonding to the αKG carboxylate group depending on whether CAD is bound or not.[16, 30, 42] In crystal structures of CAD-bound FIH where either αKG (PDB ID 1H2L) or *N*-oxalylglycine (PDB ID 1H2K) are coordinated to Fe^{II} (*N*-oxalylglycine is an inhibitor which is structurally similar to αKG and coordinates to Fe^{II} through carboxylate and α-amide carbonyl oxygens), the carboxylate of the coordinated αKG/*N*-oxalylglycine H-bonds with Asn205 and Asn294 of FIH as shown in Figure 5A. Alternatively, in structures of FIH where αKG (or a structural analog) is bound but substrate is not these H-bonds appear to be weakened or absent (see Supporting Info). This reduced H-bonding relative to the CAD-bound forms appears to relate to the conformational flexibility of FIH residues Asn205, Asn294 and Trp296 (see Supporting Info). The flexibility of Trp296 and the asparagines appears to weaken the H-bonds to the aKG carboxylate, but upon binding substrate these residues are held in a configuration where the H-bonding is stronger. When Asn205 and Asn294 were added to the 5C FIH computational model in their 1H2L locations (Figure 5A), the MLCT transition was lowered in energy by ≈ 900 cm^{-1} (Table 2D). This MLCT energy decrease combined with the fact that the calculations significantly overestimate the increase in MLCT energy upon water loss suggest that the increase in H-bonds to the αKG carboxylate provide an explanation for the observed shifts in MLCT transition energy for FIH. That the energy of the 5C FIH MLCT is higher than that of 5C TauD by ≈ 800 cm^{-1} experimentally (compare green with purple in Figure 3) is consistent with the asparagines of FIH being neutral and stabilizing the αKG **π*** orbital less than the positively-charged arginine present in TauD and CS2. Consistent with the above explanation, in variants where Asn205 or Asn294 were mutated into alanine (N205A and N294A) the MLCT is shifted up in energy by ≈ 500 cm^{-1}.[17] The stabilization of the αKG **π*** orbital through H-bonding would enhance active site reactivity with O_2, as discussed below.

Discussion

Although crystallographic studies of (Fe^{II}/αKG)FIH and spectroscopic studies of (Co^{II}/αKG)FIH indicated that the enzyme could possess a 5C site in the presence of cofactor but absence of CAD, Δour MCD spectroscopic results show that in solution (Fe^{II}/αKG)FIH does not have a 5C component. This MCD spectroscopic finding for the αKG–bound site is in agreement with the general mechanistic strategy observed for mononuclear nonheme ferrous enzymes, where an open coordination position for O_2 binding is not available until both the substrate and cofactor supplying extra electrons are in their correct positions.[4] If a significant fraction of αKG-bound Fe^{II} sites were to be 5C in the absence of substrate, uncoupled αKG turnover could take place, which would lead to autooxidation/hydroxylation and deactivation of the enzyme.

The MCD spectrum of (Fe^{II}/αKG/CAD)FIH shows that in the presence of αKG and substrate the Fe^{II} site is a mixture of 6C and 5C forms, again in accordance with our results for other α-keto-acid-dependent enzymes. This result suggests that the site is fine-tuned to release the aquo ligand from the Fe^{II} center upon substrate binding, but not to the extent that steric crowding prevents O_2 accessibility.

The facial triad carboxylate of FIH has a second-sphere interaction with its Arg238 residue (Figure 1). Removal of Arg238 from the active site of CAD-unbound FIH in computational models led the facial triad carboxylate to switch from mono- to bidentate coordination

(Figure 4D), resulting in a significant weakening of the Fe^{II} – αKG carbonyl bond. The functional significance of this residue is shown in activity assays, where the R238M mutant was inactive.[17]

These computational findings have strong implications for other aKG-dependent enzymes. Conversion to this bidentate form would limit O_2 reactivity as the bidentate carboxylate would block the coordination position of the Fe^{II}, and the longer, weaker Fe – αKG carbonyl bond would make formation of the Fe^{IV}-peroxo bridge[43] and subsequent formation of an Fe^{IV}-oxo species[44-46] difficult and together greatly increase the reaction energy barrier. Therefore, for αKG-dependent enzymes it appears crucial to avoid bidentate coordination by the facial triad carboxylate once the coordinated H_2O is lost. To determine if other members of the αKG-dependent family have counterparts to FIH Arg238 which would prevent bidentate carboxylate coordination, crystal structures for a number of the αKG-dependent enzymes were analyzed as presented in Table 3.[40, 47-51] All of the structures show an enzyme residue positioned to H-bond with the facial triad carboxylate, which thus remains monodentate upon αKG and substrate binding and leaves an open coordination site for catalysis.

These findings prompted us to extend our study of crystal structures to other nonheme Fe^{II} enzyme families in order to determine if they had similar H-bond partners as well. The results of this analysis are included in Table 3.

Like the αKG-dependent enzymes, members of the extradiol dioxygenase family possess H-bonding partners for the facial triad carboxylate, keeping the latter monodentate.[52-54] Both families require their electron sources to bind Fe^{II} in a bidentate fashion (in the case of the extradiol dioxygenases, as well as α-keto-acid-dependent HPPD and HMaS, the substrate also provides the electron source). This ligation requirement combined with the need for an open coordination position for O_2 to bind and be activated by Fe^{II} means that members of these families need three of the six Fe^{II} coordination sites available for cofactor/redox-active substrate and O_2 binding as shown in Figure 6A by orange squares.

With the two histidines of the facial triad taking one coordination site each, the facial triad carboxylate must remain mnodentate in order for O_2–activated catalysis to occur.

Alternatively, members of the pterin-dependent hydroxylases and Rieske dioxygenases generally do not have an amino acid for H-bonding with the facial triad carboxylate, and thus for these classes of nonheme Fe^{II} enzymes this residue tends to coordinate to Fe in a bidentate fashion when substrate and cofactor are present as shown in Table 3.[55-62] In pterin-dependent hydroxylases the tetrahydrobiopterin cofactor binds in the active site pocket in close proximity but not directly to the Fe^{II}, while in Rieske dioxygenases the Rieske cluster and mononuclear active site are connected to each other by an H-bond network rather than being covalently linked. In these classes of nonheme iron enzymes it is beneficial to limit the number of available sites for O_2 coordination by having the facial triad carboxylate bind in a bidentate fashion as shown in Figure 6B. In the case of the pterin-dependent hydroxylases, the Fe^{IV}=O formed from a putative Fe^{II}–O_2–BH_4 bridged species must be in a position where it can attack the π cloud of the substrate. For Rieske dioxygenases, O_2 is found to coordinate to Fe in a side-on bidentate fashion in the crystal structures of an indole–bound naphthalene dioxygenase Fe–O_2 intermediate (PDB ID 1O7N)[57] as well as a carbazole–bound carbazole 1,9a–dioxygenase Fe-O_2 intermediate (PDB ID 3VMI).[63] This side-on O_2–Fe orientation facilitates formation of the *cis*–hydroxylated product as two oxygens are poised to react with substrate. Bidentate facial triad carboxylate coordination can therefore be desirable in families of enzymes where the cofactor does not coordinate to Fe^{II} to direct proper O_2 reactivity.

(Fe^{II}/αKG)FIH Δshows a MLCT energy of 20700 cm^{-1}, which is higher than those observed for other αKG-dependent enzymes (approximately 19000 cm^{-1}). Also, binding of CAD substrate caused the MLCT to decrease to 20000 cm^{-1}, which is the opposite trend of that observed for other members of the family (for (Fe^{II}/αKG)TauD the MLCT energy is 18800 cm^{-1} which increases to 19200 cm^{-1} upon binding taurine). An increase in MLCT energy upon substrate binding is calculated and expected, as there is concomitant water loss which leads to an increase in Fe^{II} Z_{eff} thus lowering of the energy of the d orbital donor manifold. However, for FIH H-bonds are formed between enzyme residues and the carboxylate of the coordinated αKG upon substrate binding which significantly lower the MLCT transition energy. This lowering of the MLCT transition energy by H-bonding to the αKG carboxylate reflects the stabilization of the αKG π* acceptor orbital in the MLCT process. This stabilization has consequences for catalysis, as the π* orbital is involved in forming the Fe^{IV}-peroxo bridge[43] which precedes the decarboxylation and formation of the reactive Fe^{IV}-oxo species.[44-46] A lower energy π* orbital would allow more favorable nucleophilic attack by an Fe^{IV}-peroxo species and thus lower the barrier for bridge formation. This second-sphere contribution to αKG activation is consistent with the fact that αKG-dependent enzymes generally have a residue or residues capable of forming H-bonds to the coordinated carboxylate of αKG.[64]

Conclusion

In summary, this study has shown that FIH follows the same 6C → 5C conversion as observed in the general mechanistic strategy of other nonheme Fe^{II} enzymes. Importantly, in classes of enzymes where substrate or cofactor binds to Fe^{II} (αKG–dependent and extradiol dioxygenase enzymes), second–sphere H-bonding by the protein is important in maintaining monodentate coordination of the facial triad carboxylate for O_2 coordination to Fe^{II}, while for the other classes of nonheme Fe^{II} enzymes (Rieske and pterin-dependent dioxygenases) bidentate carboxylate coordination is likely important in directing O_2 reactivity. Finally, it has been shown that the enzyme second–sphere interactions contribute to coordinated αKG activity whereby H–bonding to its carboxylate stabilizes its π* LUMO for attack by the Fe^{IV}-peroxo in generating the Fe^{IV}=O intermediate.

Supplementary Material

Refer to Web version on PubMed Central for supplementary material.

Acknowledgments

This research was supported by NIH Grant GM 40392 (E.I.S.) and GM 077413 (M.J.K.). K.M.L. was also supported by the Althouse Stanford Graduate Fellowship; J.A.H. was supported by the CBI Training Grant (NIH T32-GM008515).

References and Footnotes

1. Solomon EI, Brunold TC, Davis MI, Kemsley JN, Lee S-K, Lehnert N, Neese F, Skulan AJ, Yang Y-S, Zhou J. Chem. Rev. 2000; 100:235–349. [PubMed: 11749238]
2. Que L, Ho RYN. Chem. Rev. 1996; 96:2607–2624. [PubMed: 11848838]
3. Schenk G, Pau MYM, Solomon EI. J. Am. Chem. Soc. 2004; 126:505–515. [PubMed: 14719948]
4. Neidig ML, Solomon EI. Chem. Commun. 2005:5843–5863.
5. Hegg EL, Que L Jr. Eur. J. Biochem. 1997; 250:625–629. [PubMed: 9461283]
6. Que L. Nat. Struct. Biol. 2000; 7:182–184. [PubMed: 10700270]
7. Koehntop KD, Emerson JP, Que L. J. Biol. Inorg. Chem. 2005; 10:87–93. [PubMed: 15739104]
8. Hampton-Smith RJ, Peet DJ. Ann. N. Y. Acad. Sci. 2009; 1177:19–29. [PubMed: 19845603]

9. Schofield CJ, Ratcliffe PJ. Nat. Rev. Mol. Cell Biol. 2004; 5:343–354. [PubMed: 15122348]
10. Semenza GL. Annu. Rev. Cell. Dev. Biol. 1999; 15:551–578. [PubMed: 10611972]
11. Semenza GL. Physiology. 2004; 19:176–182. [PubMed: 15304631]
12. Metzen E, Ratcliffe PJ. Biol. Chem. 2004; 385:223–230. [PubMed: 15134335]
13. McNeill LA, Hewitson KS, Claridge TD, Seibel JF, Horsfall LE, Schofield CJ. Biochem. J. 2002; 367:571–575. [PubMed: 12215170]
14. Lando D, Peet DJ, Whelan DA, Gorman JJ, Whitelaw ML. Science. 2002; 295
15. Hewitson KS, McNeill LA, Riordan MV, Tian Y-M, Bullock AN, Welford RW, Elkins JM, Oldham NJ, Bhattacharya S, Gleadle JM, Ratcliffe PJ, Pugh CW, Schofield CJ. J. Biol. Chem. 2002; 277:26351–26355. [PubMed: 12042299]
16. Elkins JM, Hewitson KS, McNeill LA, Seibel JF, Schlemminger I, Pugh CW, Ratcliffe PJ, Schofield CJ. J. Biol. Chem. 2003; 278:1802–1806. [PubMed: 12446723]
17. Saban E, Chen Y-H, Hangasky JA, Taabazuing CY, Holmes BE, Knapp MJ. Biochem. 2011; 50:4733–4740. [PubMed: 21456582]
18. Ehrismann D, Flashman E, Genn DN, Mathioudakis N, Hewitson KS, Ratcliffe PJ, Schofield CJ. Biochem.. J. 2007; 401:227–234. [PubMed: 16952279]
19. Zhou J, Gunsior M, Bachmann BO, Townsend CA, Solomon EI. J. Am. Chem. Soc. 1998; 120:13539–13540.
20. Ryle MJ, Padmakumar R, Hausinger RP. Biochem. 1999; 38:15278–15286. [PubMed: 10563813]
21. Matthews ML, Krest CM, Barr EW, Vaillancourt FH, Walsh CT, Green MT, Krebs C, Bollinger JM Jr. Biochem. 2009; 48:4331–4343. [PubMed: 19245217]
22. Chow MS, Eser BE, Wilson SA, Hodgson KO, Hedman B, Fitzpatrick PF, Solomon EI. J. Am. Chem. Soc. 2009; 131:7685–7698. [PubMed: 19489646]
23. Ryle MJ, Liu A, Muthukumaran RB, Ho RYN, Koehntop KD, McCracken J, Que L Jr. Hausinger RP. Biochem. 2003; 42
24. Henshaw TF, Feig M, Hausinger RP. J. Inorg. Biochem. 2004; 98:856–861. [PubMed: 15134932]
25. Chen Y-H, Comeaux LM, Herbst RW, Saban E, Kennedy DC, Maroney MJ, Knapp MJ. J. Inorg. Biochem. 2008; 102:2120–2129. [PubMed: 18805587]
26. Zhou J, Rocklin AM, Lipscomb JD, Que L Jr. Solomon EI. J. Am. Chem. Soc. 2002; 124:4602–4609. [PubMed: 11971707]
27. Rocklin AM, Kato K, Liu H, Que L Jr. Lipscomb JD. J. Biol. Inorg. Chem. 2004; 9:171–182. [PubMed: 14714198]
28. Neidig ML, Brown CD, Light KM, Fujimori DG, Nolan EM, Price JC, Barr EW, Bollinger JM Jr. Krebs C, Walsh CT, Solomon EI. J. Am. Chem. Soc. 2007; 129:14224–14231. [PubMed: 17967013]
29. To be published.
30. Dann CE III, Bruick RK, Diesnhofer J. Proc. Natl. Acad. Sci. U. S. A. 2002; 99:15351–15356. [PubMed: 12432100]
31. Solomon EI, Pavel EG, Loeb KE, Campochiaro C. Coord. Chem. Rev. 1995; 144:369–460.
32. Pavel EG, Kitajima N, Solomon EI. J. Am. Chem. Soc. 1998; 120:3949–3962.
33. Pavel EG, Zhou J, Busby RW, Gunsior M, Townsend CA, Solomon EI. J. Am. Chem. Soc. 1998; 120:743–753.
34. Zhou J, Kelly WL, Bachmann BO, Gunsior M, Townsend CA, Solomon EI. J. Am. Chem. Soc. 2001; 123:7388–7398. [PubMed: 11472170]
35. Frisch, MJ., et al. Gaussian 09 Revision A.1. Gaussian, Inc.; Wallingford, CT: 2009.
36. Tomasi J, Mennucci B, Cammi R. Chem. Rev. 2005; 105:2999–3093. [PubMed: 16092826]
37. Neidig ML, Decker A, Choroba OW, Huang F, Kavana M, Moran GR, Spencer JB, Solomon EI. Proc. Natl. Acad. Sci. U. S. A. 2006; 103:12966–12973. [PubMed: 16920789]
38. Hegg EL, Whiting AK, Saari RE, McCracken J, Hausinger RP, Que L Jr. Biochem. 1999; 38:16714–16726. [PubMed: 10600135]
39. Wick CR, Lanig H, Jäger CM, Burzlaff N, Clark T. Eur. J. Inorg. Chem. 2012; (31):4973–4985.

40. Zhang Z, Ren J, Stammers DK, Baldwin JE, Harlos K, Schofield CJ. Nature Struct. Biol. 2000; 7:127–133. [PubMed: 10655615]
41. O'Brien JR, Schuller DJ, Yang VS, Dillard BD, Lanzilotta WN. Biochem. 2003; 42:5547–5554. [PubMed: 12741810]
42. Conejo-Garcia A, McDonough MA, Loenarz C, McNeill LA, Hewitson KS, Ge W, Liénard BM, Schofield CJ, Clifton IJ. Bioorg. Med. Chem. Lett. 2010; 20:6125–6128. [PubMed: 20822901]
43. Diebold AR, Brown-Marshall CD, Neidig ML, Brownlee JM, Moran GR, Solomon EI. J. Am. Chem. Soc. 2011; 133:18148–18160. [PubMed: 21981763]
44. Price JC, Barr EW, Tirupati B, Bollinger JM Jr. Krebs C. Biochem. 2003; 42:7497–7508. [PubMed: 12809506]
45. Price JC, Barr EW, Glass TE, Krebs C, Bollinger JM Jr. J. Am. Chem. Soc. 2003; 125:13008–13009. [PubMed: 14570457]
46. Hoffart LM, Barr EW, Guyer RB, Bollinger JM Jr. Krebs C. Proc. Natl. Acad. Sci. U. S. A. 2006; 103:14738–14743. [PubMed: 17003127]
47. Yu B, Hunt JF. Proc. Natl. Acad. Sci. U. S. A. 2009; 106:14315–14320. [PubMed: 19706517]
48. Wilmouth RC, Turnbull JJ, Welford RWD, Clifton IJ, Prescott AG, Schofield CJ. Structure. 2002; 10:93–103. [PubMed: 11796114]
49. Clifton IJ, Sleeman MC, Topf M, Suzuki H, Wilmouth RC, Schofield CJ. J. Biol. Chem. 2003; 278:20843–20850. [PubMed: 12611886]
50. Yang C, Pflugrath JW, Camper DL, Foster ML, Pernich DJ, Walsh TA. Biochem. 2004; 43:10414–10423. [PubMed: 15301540]
51. Brownlee J, He P, Moran GR, Harrison DH. Biochem. 2008; 47:2002–2013. [PubMed: 18215022]
52. Sato N, Uragami Y, Nishizaki T, Takahashi Y, Sazaki G, Sugimato K, Nonaka T, Masai E, Fukuda M, Senda T. J. Mol. Biol. 2002; 321:621–636. [PubMed: 12206778]
53. Kovaleva EG, Lipscomb JD. Science. 2007; 316:453–457. [PubMed: 17446402]
54. Vetting MW, Wackett LP, Que L, Lipscomb JD, Ohlendorf DH. J. Bacteriol. 2004; 186:1945–1958. [PubMed: 15028678]
55. Andersen OA, Flatmark T, Hough E. J. Mol. Biol. 2001; 314:279–291. [PubMed: 11718561]
56. Andersen OA, Stokka AJ, Flatmark T, Hough E. J. Mol. Biol. 2003; 333:747–757. [PubMed: 14568534]
57. Karlsson A, Parales JV, Parales RE, Gibson DT, Eklund H, Ramaswamy S. Science. 2003; 299:1039–1042. [PubMed: 12586937]
58. Colbert CL, Agar NY, Kumar P, Chakko MN, Sinha SC, Powlowski JB, Eltis LD, Bolin JT. PLoS ONE. 2013; 8 Online. Article e52550. http://www.plosone.org/article/info%3Adoi%2F10.1371%2Fjournal.pone.0052550.
59. In addition, the pterin-dependent enzyme Tyrosine Hydroxylase was shown through EXAFS to have bidentate carboxylate coordination when both tetrahydrobiopterin and substrate are bound. See (22).
60. A possible exception is the Rieske dioxygenase family member Carbazole Dioxygenase, which has an asparagine available for H-bonding to the facial triad carboxylate and carboxylate O – Fe^{II} bond lengths of ≈ 2.0 and 2.7 Å. See (61), (62).
61. Nojiri H, Ashikawa Y, Noguchi H, Nam J-W, Urata M, Fujimoto Z, Uchimura H, Terada T, Nakamura S, Shimizu K, Yoshida T, Habe H, Omori T. J. Mol. Biol. 2005; 351:355–370. [PubMed: 16005887]
62. Ashikawa Y, Fujimoto Z, Noguchi H, Habe H, Omori T, Yamane H, Nojiri H. Structure. 2006; 14:1779–1789. [PubMed: 17161368]
63. Ashikawa Y, Fujimoto Z, Usami Y, Inoue K, Noguchi H, Yamane H, Nojiri H. BMC Struct. Biol. 2012; 12 Online. Article 15. http://www.biomedcentral.com/1472-6807/12/15.
64. Hangasky JA, Taabazuing CY, Valliere MA, Knapp MJ. Metallomics. [Online early access]. DOI: 10.1039/C3MT20153H. Published Online: Jan. 24, 2013. http://pubs.rsc.org/en/content/articlelanding/2013/mt/c3mt20153h.

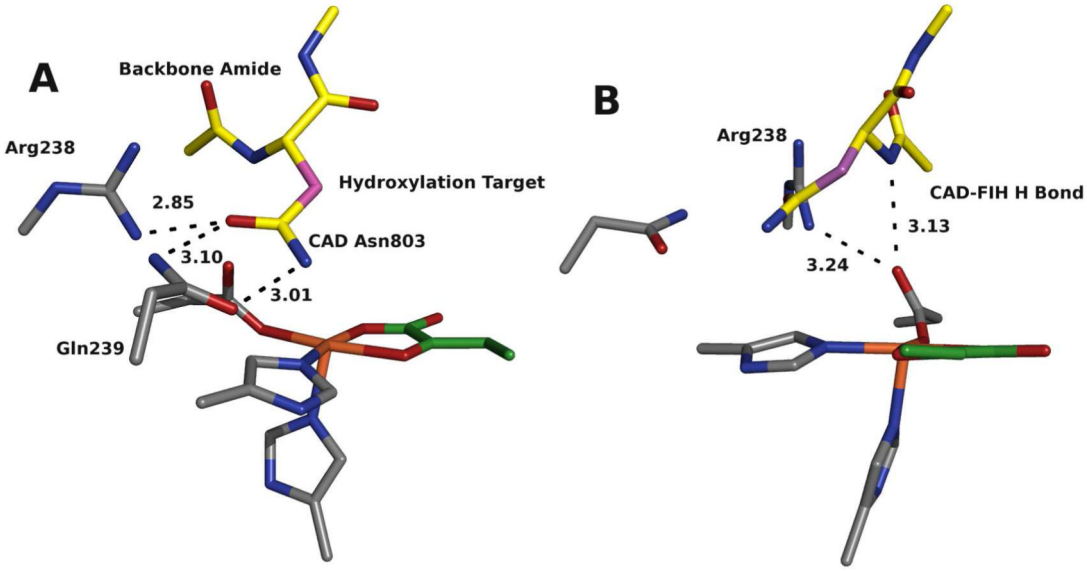

Figure 1.

Views of the CAD-bound FIH Fe^{II} active site from crystal structure 1H2L showing *(A)* H-bonds between the CAD Asn803 amide and the FIH residues Arg238 and Gln239, and *(B)* H-bonds between the FIH facial triad carboxylate and FIH Arg238 and the CAD Val802-Asn803 backbone amide. The C atoms of the FIH and CAD residues are colored grey and yellow, respectively, with the exception of the site of CAD hydroxylation, which is colored magenta. The C atoms of the bound αKG are colored green (the carboxylate tail has been removed). All distances are in Å.

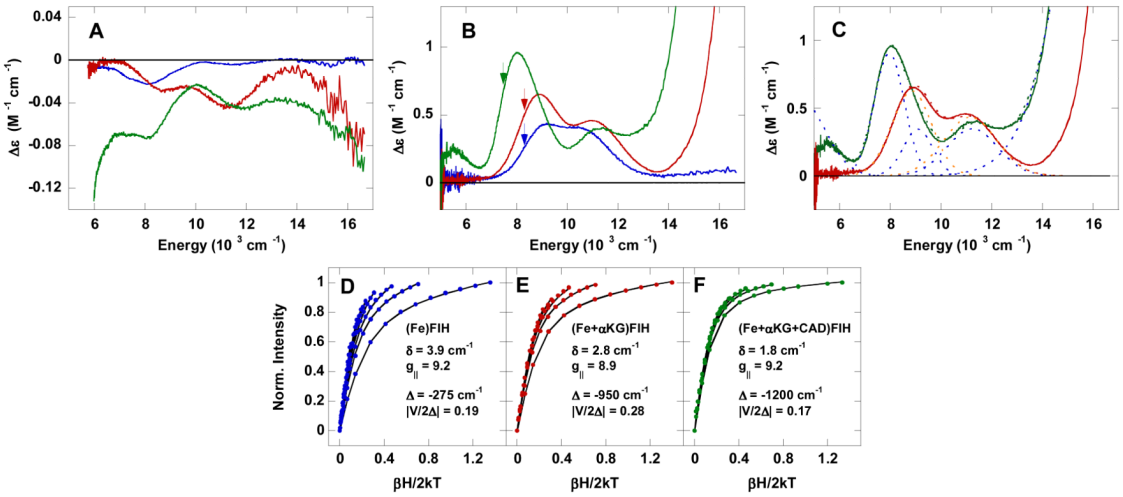

Figure 2.

NIR CD, MCD, and VTVH MCD spectra of FIH. *(A)* The 283 K CD spectra of FIH/Fe^{II} (blue), FIH/Fe^{II}/αKG (red), and FIH/Fe^{II}/αKG/CAD (green). *(B)* The low temperature (1.8 K for FIH/Fe^{II} and FIH/Fe^{II}/αKG, 3 K for FIH/Fe^{II}/αKG/CAD), 7 T MCD spectra of FIH/Fe^{II} (blue), FIH/Fe^{II}/αKG (red), and FIH/Fe^{II}/αKG/CAD (green). Arrows indicate energies for which VTVH data were collected for each sample. *(C)* The MCD spectra of FIH/Fe^{II}/αKG (red) and FIH/Fe^{II}/αKG/CAD (green) with best fits (red dashed for FIH/Fe^{II}/αKG and green dashed for FIH/Fe^{II}/αKG/CAD) and their component peaks (orange, dashed for FIH/Fe^{II}/αKG and blue, dashed for FIH/Fe^{II}/αKG/CAD). VTVH data (symbols) and best fits (lines) for FIH/Fe^{II} *(D)*, FIH/Fe^{II}/αKG *(E)*, and FIH/Fe^{II}/αKG/CAD *(F)*.

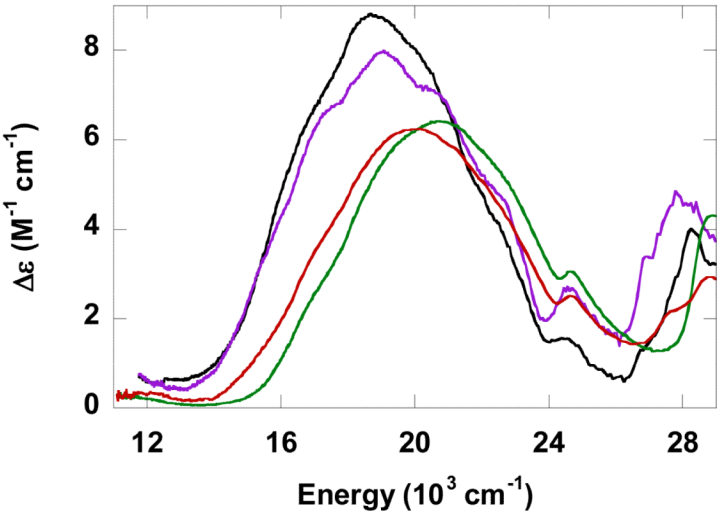

Figure 3.
Vis-UV MCD spectra of αKG-bound FIH (red) and αKG/CAD-bound FIH (green) compared with αKG-bound TauD (black) and αKG/taurine-bound TauD (purple).

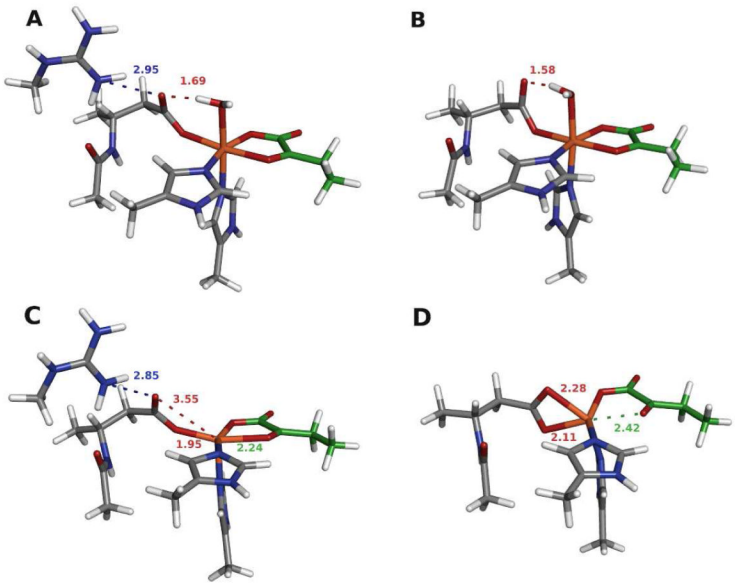

Figure 4.

DFT optimized structures of FIH, showing the effects of Arg238 displacement on 6C (*(A)* and *(B)*) and 5C (*C)* and *(D)*) forms. Arg-238-facial triad carboxylate heavy atom distance in blue, facial triad carboxylate O-Fe^{II} and O-H distances in red, and αKG carbonyl O-Fe^{II} distance in green. All distances are measured in Å.

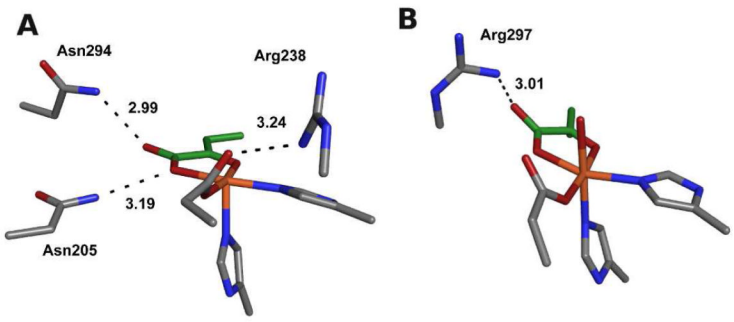

Figure 5.

αKG H-bonding effects on MLCT. *(A)* Crystal structure of CAD-bound FIH with Arg238, showing H-bonds between the αKG carboxylate and FIH residues Asn205 and Asn294. *(B)* Crystal structure of Clavaminate Synthase showing an H-bond between the αKG carboxylate and Arg297. All distances are in Å.

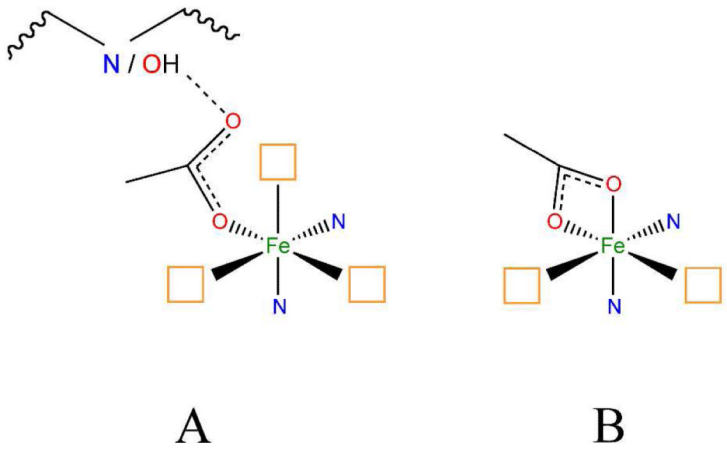

Figure 6.

Fe^{II} site geometries for (A) αKG-dependent and extradiol dioxygenases, and (B) pterin-dependent and Rieske dioxygenases. Orange squares denote coordination sites available for cofactor and O_2.

Table 1

^5E_g energy splittings, VTVH parameters and ground state parameters for FIH and CS2 species.

	Fe^{II} FIH	Fe^{II} CS2[a]	Fe^{II}/αKG FIH	Fe^{II}/αKG CS2[a]	Fe^{II}/αKG/CAD FIH[b]	Fe^{II}/αKG/DGPC CS2[b,d]
Δ^5E_g (cm^{-1})	1800	1690	2300	1630	> 3000[c]	3600
δ (cm^{-1})	3.9	4.5	2.8	2.7	1.8	2.1
$g_{\|\|}$	9.2	9.2	8.9	8.7	9.2	8.8
Δ (cm^{-1})	−275	−400	−950	−1000	−1200	−1300
$\|V/2\Delta\|$ (cm^{-1})	0.19	0.24	0.28	0.33	0.17	0.27
$\|V\|$ (cm^{-1})	100	190	530	670	410	800

[a] Data taken from ref. 26.

[b] Data for the 5C component.

[c] Cannot be exactly determined as λ_{max} of low-energy peak is not observed.

[d] Data taken from ref. 28.

Table 2

TD-DFT energies for the Fe-αKG π* MLCT of various models to show the effects of αKG carboxylate H-bonding. *(A)* The MLCT effect of shifting Arg 238 to the CS2/Taud Position. *(B)* The effect of water loss from the FIH model. *(C)* The effect of water loss from the CS2/TauD model. *(D)* The combined effects of water loss and addition of Asn205 and Asn294-αKG carboxylate H-bonds.

	Form	MLCT[a]
A	Arg in FIH position, 6C Arg in CS2/TauD position, 6C	13100 10600
	Difference (Arg in CS2/TauD pos.)	−2500
B	Arg in FIH position, 6C Arg in FIH position, 5C	13100 14800
	Difference (Remove H_2O, FIH)	1700
C	Arg in CS2/TauD position, 6C Arg in CS2/TauD position, 5C	10600 12100
	Difference (Lose H_2O, CS2/TauD)	1500
D	Arg in FIH position, 6C Arg in FIH position, 5C, with Asns	13100 13900
	Difference (Lose H_2O, add Asn's)	800

[a] All energies are in cm^{-1}.

Table 3

Enzyme-based H-bonding partners for the facial triad carboxylate and facial triad carboxylate O-Fe bond distances for members of the 4 mononuclear nonheme Fe enzyme families.

Family	Enzyme	Form	PDB ID[a]	H-Bonding Residue(s) (Distance, Å)	Fe-RCO_2 Distances (Å)
αKG-Dependent	Clavaminate Synthase	Fe/αKG Fe/αKG/PC	1DS1[40] 1DRT[40]	Y299 (2.68) Y299 (2.72)	2.06, 3.39 2.07, 3.44
	AlkB	Mn/αKG Fe/αKG/DNA	3I3Q[47] 3I2O[47]	R210 (2.86, 2.87) R210 (2.87, 2.87)	2.14, 3.37 2.09, 3.24
	Anthocyanidin Synthase	Fe/αKG/AN	1GP5[48]	T239 (2.88)	2.25, 3.33
	Carbapenum Synthase	Fe/αKG Fe/αKG/N7P	1NX4[49] 1NX8[49]	Q269 (3.10) Q269 (3.10)	2.07, 3.00 2.10, 3.30
	HPPD	Fe Fe/869B Inhib.	1SQD[50] 1TFZ50	Q358 (2.71) Q358 (2.76)	2.17, 3.78 2.02, 3.46
	HMaS	Fe/4-OH MA	2R5V[51]	Q305 (2.68)	2.10, 3.59
Extradiols	2,3-DHBPD	Fe Fe/DHBP	1KW3[52] 1KW6[52]	S247 (2.81) S247 (2.72), H240 (2.66)	2.01, 3.57 1.99, 3.70
	HPCD	Fe Fe/HPC	2IG9[53] 1Q0C[54]	H248 (2.77) H248 (2.80)	2.05, 3.58 2.07, 3.58
Pterin-Dependent	Phenylalanine Hydroxylase	Fe/BH4 Fe/BH4/Thyl Ala Fe/BH4/Norleucine	1J8U[55] 1MMK[56] 1MMT[56]	N/A N/A N/A	2.06, 3.15 2.43, 2.44 2.29, 2.40
Rieske	Naphthalene Dioxygenase	Fe Fe/Naphthalene	107W[57] 1O7G[57]	N/A N/A	2.27, 2.38 2.26, 2.43
	Biphenyl Dioxygenase	Fe Fe/Biphenyl	3GZY[58] 3GZX[58]	N/A N/A	1.97, 2.38 2.23, 2.45
	Carbazole Dioxygenase	Fe Fe/Carbazole	1WW9[61] 2DE7[62]	N330 (2.86) N330 (2.70)	2.10, 2.70 2.00, 2.70

[a]Citations given as superscripts.